Free Radical Biology and Medicine 232 (2025) 340–352

Contents lists available at ScienceDirect

Free Radical Biology and Medicine

journal homepage: www.elsevier.com/locate/freeradbiomed

Astragalin alleviates lipopolysaccharide-induced depressive-like behavior in mice by preserving blood-brain barrier integrity and suppressing neuroinflammation

Min-Min Cao [a,1], Zhe Guo [b,1], Jun Wang [a], Hui-Yong Ma [a], Xiao-Yan Qin [a,*], Yang Hu [a,**], Rongfeng Lan [c,***]

[a] Key Laboratory of Ecology and Environment in Minority Areas National Ethnic Affairs Commission, Center on Translational Neuroscience, College of Life and Environmental Sciences, Minzu University of China, Beijing, 100081, China
[b] The Emergency Department, The Third Affiliated Hospital of Guangxi Medical University, Nanning, 530021, China
[c] Department of Cell Biology & Medical Genetics, School of Basic Medical Sciences, Shenzhen University Medical School, Shenzhen, 518060, China

ARTICLE INFO

Keywords:
Astragalin
RIPK1
mTOR
IBA1
LPS

ABSTRACT

Astragalin (AST) is a flavonoid glycoside commonly found in edible plants and medicinal herbs with a variety of therapeutic effects. This study aimed to investigate whether AST protects the integrity of the blood-brain barrier (BBB) and inhibits neuroinflammation, thereby alleviating depressive-like behaviors. LPS-stimulated cultured cells and LPS-induced BBB disruption and depressive-like behavior mice models were employed. We founded that AST inhibited LPS-induced inflammatory responses in microglial BV2 cells and protected SH-SY5Y cells from inflammatory injury. In mice, AST effectively ameliorated LPS-induced depressive-like behaviors, which was attributed to its ability to maintain BBB integrity and inhibit inflammatory damage caused by LPS invasion. Furthermore, AST suppressed LPS-induced activation of glial cells, protecting neuronal dendritic spines, synapses, and mitochondria from inflammatory damage. It also reduced the elevation of pro-inflammatory factors such as TNF-α, IL-1β, and IL-6, and normalized the aberrant activation of inflammatory signaling pathways, including RIPK1/RIPK3/MLKL and mTOR/NF-κB. In conclusion, AST protects BBB integrity and brain tissue from inflammatory damage, offering new insights for drug development and clinical interventions in systemic inflammatory responses, such as sepsis-induced encephalitis.

Abbreviations: ALT, Alanine aminotransferase; ANOVA, analysis of variance; AST, Astragalin; BBB, Blood-brain barrier; BDNF, brain derived neurotrophic factor; CAT, Catalase; CNS, Central nervous system; DAPI, 4′ 6-diamidino-2-phenylindole; DMEM, Dulbecco's modified eagle medium; EB, Evans blue; ELISA, Enzyme-linked immunosorbent assay; G6pdx, Glucose-6-phosphate dehydrogenase X-linked; GFAP, Glial fibrillary acidic protein; Glut1, glucose transporter 1; HIF-1α, Hypoxia-inducible factor-1α; HK, hexokinase; IBA1, Ionized calcium-binding adaptor molecule-1; IF, Immunofluorescences; IL-6, Interleukin-6; IL-1β, Interleukin-1β; IM, Inflammatory medium; LA, L-lactic acid; LDHA, Lactate dehydrogenase A; LPS, Lipopolysaccharide; MAP2, Microtubule associated protein 2; MDA, Malondialdehyde; MMP9, Matrix metalloproteinase 9; NES, neuron-specific enolase; OFT, Open field test; PBS, Phosphate buffered saline; PKM2, Pyruvate kinase M2; RIPK1, Receptor-interacting serine/threonine-protein kinase 1; RIPK3, Receptor-interacting serine/threonine-protein kinase 3; MLKL, Mixed lineage kinase domain-like protein; mTOR, Mammalian target of rapamycin (mTOR); NF-κB, Nuclear factor kappa B; SAE, sepsis-associated encephalopathy; SOD, Superoxide dismutase; SPT, Sucrose preference test; SYN1, Synapsin-1; SYP, Synaptophysin; PDH, Pyruvate dehydrogenase; PK, Pyruvate kinase; PSD95, Postsynaptic density protein 95; T-AOC, Total antioxidant capacity; TBK1, TANK-binding kinase 1; TEM, Transmission electron microscope; TNF-α, Tumor necrosis factor alpha; TST, Tail suspension test.

* Corresponding author.
** Corresponding author.
*** Corresponding author.
E-mail addresses: bjqinxiaoyan@muc.edu.cn (X.-Y. Qin), yang.hu@muc.edu.cn (Y. Hu), lan@szu.edu.cn (R. Lan).
[1] These authors contribute equally: M-M. Cao, and Z. Guo.

https://doi.org/10.1016/j.freeradbiomed.2025.03.014
Received 3 January 2025; Received in revised form 25 February 2025; Accepted 11 March 2025
Available online 13 March 2025

1. Introduction

The blood-brain barrier (BBB) is a physiological defence system that separates the brain from the peripheral circulatory system. It selectively prevents the entry of nonessential and harmful substances while facilitating the transport of essential nutrients to the central nervous system (CNS) [1]. This barrier is essential for maintaining normal CNS function. However, it can be severely compromised during pathogen attacks or systemic inflammation, such as when lipopolysaccharides (LPS) from Gram-negative bacteria invade the circulatory system. LPS administration triggers systemic inflammation, leading to BBB breakdown and the infiltration of peripheral immune cells and pro-inflammatory cytokines into the brain. This neuroinflammatory response disrupts neuronal homeostasis, particularly in regions critical for mood regulation, such as the hippocampus and prefrontal cortex. Such disruptions may contribute to the development of neurological disorders, including sepsis-associated encephalopathy (SAE), which is associated with poor prognosis and high mortality rates [2]. Therefore, elucidating the mechanisms by which LPS disrupts the BBB and identifying potential therapeutic interventions could have significant clinical implications. Restoring BBB integrity and suppressing neuroinflammation may provide novel strategies for treating SAE. In experimental studies, LPS-induced BBB injury in animal models often results in depressive-like behavioral phenotypes [3,4], characterized by reduced mobility, impaired synaptic plasticity, and altered neurogenesis [5,6]. These models are thus valuable for studying depression and developing therapeutic agents. At the cellular and molecular levels, glial cell hyperactivation and neuronal damage are common, with LPS-treated mouse hippocampal neurons showing reduced dendritic spines and altered synaptic structures [7]. LPS binding to Toll-like receptor 4 (TLR4) on microglia induces a pro-inflammatory M1 phenotype, leading to the release of inflammatory factors that inhibit neuronal activity and cause neuronal loss [8,9]. Intracellularly, enzymes involved in glycolysis become highly active, inhibiting apoptosis while activating the receptor-interacting serine/threonine-protein kinase (RIPK1) mediated signaling axis, leading to mixed lineage kinase domain-like protein (MLKL) phosphorylation and membrane disruption [10,11].

AST, a flavonoid glycoside found in medicinal plants, vegetables, a and fruits, is a kaempferol O-glucoside with anti-inflammatory, antioxidant, and antibacterial properties [12–14]. Named after *Astragalus sinicus* L., which is recorded in Pen-tsao Kan-mu for treating hepatitis, conjunctivitis, and neuralgia, AST has shown promise in previous studies. We reported that AST ameliorated learning and memory deficits in mice induced by $AlCl_3$/D-Gal, particularly protecting hippocampal neurons [15]. Earlier this year, we found that AST protected mice from acute liver injury caused by LPS, attenuating oxidative stress and inflammation [16]. Additionally, AST alleviated depressive-like behavior in LPS-treated mice. This study investigates AST's anti-inflammatory and neuroprotective effects using LPS-induced cell and mouse models, focusing on its ability to protect the BBB and neuronal dendritic spines and synapses from LPS-induced damage. The goal is to explore the potential of natural compounds like AST, with broad anti-inflammatory and antioxidant properties, in neurological drug discovery.

2. Materials and methods

2.1. Animals and ethics

Forty 15-week-old male BALB/C mice, 25–30 g, were purchased from Beijing Vital River Laboratory Animal Technology Co., Ltd., Batch No. SCXK2021-0013. Animals were housed in an environment with a room temperature of 23 ± 2 °C, relative humidity of 40 %–70 %, and a 12-h light-dark cycle, with free food and water. After a 7-day acclimatization period, experiments were conducted in accordance with the Beijing Municipal Regulations on the Management of Laboratory Animals and were approved by the Ethics Committee of Minzu University of China on March 12, 2022 (No. ECMUC2022002AA).

2.2. LPS-induced depressive-like model in mice

BALB/C mice were randomly divided into Control, LPS, LPS + AST, and AST groups (n = 10). On day 1, mice were gavaged with saline or AST (10 mg/kg body weight), and 1 h later, LPS (2.5 mg/kg body weight) was injected intraperitoneally in the LPS group and LPS + AST group, while the Control group was injected with an equal amount of saline. The procedure was repeated on day 2. Behavioural tests were conducted from day 3 to day 5. On day 6, mice were anesthetized with isoflurane for blood and brain tissue collection [17]. For brain isolation, anesthetized mice were secured on a dissection table. The scalp and skull were incised to expose the brain, and brain tissue was carefully extracted from the cranial cavity using forceps, ensuring no damage during the process. The extracted brain was placed in a brain sectioning mold, and the hippocampus or other regions were identified. Isolated tissues were immediately placed in pre-cooled 4 % paraformaldehyde for fixation or frozen at −80 °C for storage.

2.3. Cell lines and reagents

AST (99.9 %, # MUST-2242912) was purchased from Chengdu Must Biotechnology Co., Ltd. LPS (#L2880, from *E. coli* O55:B5) was obtained from Sigma-Aldrich. SH-SY5Y (human neuroblastoma cells) and BV2 (mouse microglia cells) were provided from the Institute of Basic Medical Sciences of the Chinese Academy of Medical Sciences. Cells were cultured in dulbecco's modified eagle medium (DMEM) supplemented with 10 % fetal bovine serum, 100 U/mL penicillin and 100 μg/mL streptomycin at 37 °C and 5 % CO_2.

2.4. Establishment of inflammatory culture

BV2 cells were stimulated with LPS (0.1, 1, 10, 20, 40 μg/mL) suspended in culture medium for 24 h, then the supernatants was collected as inflammatory medium (IM) [18], and centrifuged at 1000 rpm for 20 min, and mixed with fresh medium (containing 10 % fetal bovine serum, 1 % penicillin/streptomycin) in a 1:1 ratio to produce inflammatory medium for SH-SY5Y cells. The cell viability was detected by using the CCK8 kit (#C0039, Shanghai Beyotime Bio-Tech Co., Ltd.) after 24 h of culture. The optimal concentration of LPS was then selected for the AST protection assay, in which gradient AST (0.2 μM, 2 μM, and 20 μM) was added.

2.5. Neurobehavioral scoring

Behavioural changes of mice in each group were observed 24 h after drug administration, and the mice were scored for reflexes to auricular, tail pinch, corneal, evasion, and flip-flop, respectively [19], with a score of 2 for normal for each item, a score of 1 for weakened reflexes (5 s < interval<10 s), a score of 0 for disappeared reflexes (intervals>10 s), and a maximum score of 10, with lower scores indicating more severe nerve damage. The lower the score, the more severe the nerve damage.

2.6. Behavioural tests

Open field test (OFT): to evaluate the mice's autonomous, nervous and exploratory behaviours in a new environment. The mice were placed in a square test box (size 50 × 50 cm). The active trajectories of mice were recorded for 5 min and statistical analysed by using the BAS-100 Animal Behaviour Analysis System (Chengdu Techman Software Co., Ltd.) to calculate the total distance and the total time of the mice in the central area [20].

Tail suspension test (TST): to measure behavioural despair or "depressive-like" behaviour and learned helplessness. Mice are taped 2

cm from the end of their tails and hung upside down with their heads 15 cm off the ground. The activity of the mice was then recorded on video for 6 min. The first minute was the acclimatization time, and the next 5 min were counted as the cumulative time that the mice remained stationary, at which time they stopped struggling and remained stationary with their bodies upside down [21].

Sucrose preference test (SPT), which measures the relative preference of rodents for sucrose and water to assess hedonic behaviour. Prior to the formal experiment, mice are subjected to a baseline test for sucrose water, and mice with abnormal baseline tests are excluded. At the beginning, two bottles containing 1 % sucrose water are available in the cage for sucrose acclimatization. After 24 h, one of the bottles is switched to drinking water, and sucrose-water switching takes place after 12h. The test was started after 12 h of fasting and water fasting, and the amount of sucrose water and normal water consumed by each mouse was counted and the preference for sucrose water was calculated according to the following formula: Percentage of sucrose water preference = Sucrose water intake/(Sucrose water intake + normal water intake) x 100 % [22].

2.7. Serum aminotransferase assay

After anaesthesia, blood was collected from the eyes, left at room temperature for 30 min to clot, and then centrifuged at 4 °C and 3000 rpm for 10 min to collect the supernatant for testing. Alanine aminotransferase (ALT/GPT) and glutamate aminotransferase (AST/GOT) were measured by ELISA kits (#C009-2-1 and #C010-2-1) from the Nanjing Jiancheng Bioengineering Institute.

2.8. Oxidative stress and serum marker assays

Brain tissues were homogenized in a volume of saline equivalent to 9 times their weight for 2 min with a high-speed tissue mill to make a 10 % homogenate, which was centrifuged at 12,000 rpm for 10 min, and the supernatant was collected for the assay. Total superoxide dismutase (SOD, #A001-1), Malondialdehyde (MDA, #A003-1), Catalase (CAT, #A007-1-1), and total antioxidant capacity (T-AOC, #A015-1) were detected in the brain homogenate and serum by using kits from Nanjing Jiancheng Institute of Bioengineering.

Measurements of L-lactic acid (LA) (#BC2235), ATP (#BC0305), and the activities of pyruvate kinase (PK) (#BC0545), hexokinase (HK) (#BC0745), pyruvate dehydrogenase (PDH) (#BC0385) and were determined in brain tissue supernatants using the kits from Beijing Solarbio Science & Technology Co., Ltd.

ELISA for the serum markers of nerve injury, neuron-specific enolase (NSE) (#ml063810) and S-100 protein subunit beta (S100β) (#ml037988), were performed by kits provided by Shanghai mlbio technology Co., Ltd.

2.9. Brain water content and BBB permeability

Twenty-four hours after drug administration, four mice in each group were randomly selected and injected with 2 % Evans blue (EB) (4 mL/kg body weight) via tail vein. Two hours later, mice were anesthetized and the left ventricle was perfused with 0.9 % saline to extract the brain. After isolation, the left brain is weighed and homogenized in formamide (10 mL/kg) for 24 h at 60 °C, then centrifuged at 3000 rpm for 30 min at 4 °C. The supernatant was collected for determination of absorbance at 630 nm. The standard curve was produced by preparing 64.000, 32.000, 16.000, 8.00, 4.000, 2.000, 1.000, 0.500, 0.250, 0.125 μg/mL of Evans blue solution using formamide solution as a blank control, and the content of Evans blue was calculated. In addition, the right brain was weighed (wet) and then baked at 80 °C for 48 h until a constant weight (dry) was obtained. Water content of brain tissue (%) = (wet weight-dry weight)/wet weight x 100 % [23].

2.10. RT-qPCR

Whole-cell RNA was extracted from brain tissues using Trizol reagent (#15596018, Shanghai Beyotime Biotechnology Co., Ltd). cDNA was synthesized from 1 μg of total RNA using the Reverse Transcription Kit (All-in-one 1st Strand cDNA Synthesis SuperMix (gDNA Purge)) (Suzhou Novoprotein, #E047-01B). A mixture of polymerase premix, primers and cDNA template for qPCR was prepared using SYBR Green PCR Master Mix (Suzhou Novoprotein, #E096-01B) and uniformly dispensed into 96-well plates. The expression of the target gene was calculated using the $2^{-\Delta\Delta Ct}$ method and normalized to β-actin. Three replicates were set up for each sample and three samples were tested with the primer sequences shown below. β-actin, 5′-TGTCCACCTTCCAGCAGA-3’ (F) and 5′-GCTCAGTAACAGTCCGCCTA-3 ’ (R); TNF-α, 5′-TGACCCCCATTACTGACC-3’ (F) and 5′-GGCCACTACTTCAGCTC-3’ (R); IL-6, 5′-ATTCTGTCTCGAGCCCACCA-3’ (F) and 5′-AGGCAACTGCTGGAAGTCT-3’ (R); IL-1β, 5 ′-AATGCCTCG TGCTGTCTGA-3’ (F) and 5′-TGTCGTTCTTGTCTCCT-3’ (R); PKM2,5′-CAGAGAAGGTCTTCCTGGCTCA-3’ (F) and 5′-GCCACATCACTGCC TTCAGCAC-3’ (R); HK2, 5′- CCCTGTGAAGATGTTGCCCACT-3’ (F) and 5′-CCTTCGCTTGCCATTACGCACG-3’ (R); Glut1, 5′- GCTTCTCCAACTG-GACCTCAAAC-3’ (F) and 5′-ACGAGGAGCACCGTGAAGATGA-3’ (R); G6pdx,5′- GACCAAGAAGCCTGGCATGTTC-3’ (F) and 5′-AGA-CATCCAGGATGAGGCGTTC-3’ (R); LDHA, 5′- ACGCAGA-CAAGGAGCAGTGGAA-3’ (F) and 5′-ATGCTCTCAGCCAAGTCTGCCA-3’ (R); HIF-1α, 5′- ACATGGGGTTAACTCAGTTTGAA-3’ (F) and 5′-AGCTCCGCTGTGTGTTTAGT-3’ (R).

2.11. Immunofluorescence staining (IF)

Brain tissues were embedded in 4 % paraformaldehyde and fixed for more than 7 days, sliced into 30 μm sections on a cryosectioning machine, and stored at −20 °C for use. For cultured cells, cells were seeded on slides in 24-well plates and fixed with 250 μL paraformaldehyde for 15 min at room temperature. For IF, the preserved sections or cell slides were rinsed 3 times with phosphate buffered saline (PBS), then incubated with 5 % goat serum albumin (containing 0.2 % Triton X-100) blocking solution for 20 min, and the primary antibody was incubated at 4 °C overnight. Slices were rinsed three times with PBS, then secondary antibody solution was added and incubated at 37 °C for 1–2 h at room temperature. After washing, slides were stained with DAPI and imaged. The antibodies were as follows: IBA1 (#019–19741, Wako); GFAP (#16825-1-AP, Proteintech), PKM2 (#60268-1-Ig, Proteintech), and MAP2 (#17490-1-AP, Proteintech).

2.12. Western blotting

Mouse brain tissues or cultured cells were lysed with lysis buffer containing phosphatase inhibitor and protease inhibitor (#P0013B, Shanghai Beyotime Biotechnology Co., Ltd.) to extract the proteins and their concentrations were determined according to the BCA kit (#P0011). Protein samples were electrophoresed on 10 % sodium dodecyl sulfate-polyacrylamide gels, transferred to polyvinylidene difluoride (PVDF) membranes, sealed with 5 % skimmed milk for 1 h at room temperature, washed three times with PBS, and then incubated with primary antibody at 4 °C overnight and with secondary antibody for 1 h at room temperature. Finally, after rinsing three times with PBS, target proteins were visualized with the ECL luminescence reagent (#P0018M) and imaged. Normalized expression levels of proteins were calculated from the band density values using Image J software. The antibodies were shown as follows, TNF-α (#17590-1-AP), HIF-1α (#20960 1-AP), PKM2 (#60268-1-Ig), β-actin (#81115-1-RR), TANK-binding kinase 1 (TBK1, #28397-1-AP), NF-κB (#10745-1-AP), BDNF (#28205-1-AP), SYN1 (#20258-1-AP), Cleaved-Caspase 3 (#66470-2-lg), mTOR (#66888-1-lg), Phospho-mTOR (Ser2448) (#67778-1-lg), MAP2 (#17490-1-AP) were from Proteintech Group, Inc. Phospho-TBK1 (Ser172) (#BD-PP1527) was from Beijing Biodragon Co., Ltd. Phospho-

RIPK1 (Ser166) (#31122S), RIPK1(#D94C12) (#3493S), RIPK3 (#D8J3L) (#15828S), Phospho-RIPK3 (# 91702S), Claudin-5 (E8F3D) (#49564S) were from Cell Signalling Technology, Inc. SYP (#AF8091) and PSD95 (#AF1096) were from Shanghai Beyotime Biotechnology Co., Ltd. And phospho-MLKL (#MABC1158, Millipore), MLKL (#PA5-71886, Thermo Fisher Scientific), Phospho-NF-κB (Ser468) (#bs-3485R, Bioss Antibodies), MMP-9 (#GTX100458, GeneTex), HRP-labelled goat anti-rabbit IgG (#ZB-2301, Beijing ZSGB-Bio), HRP-labelled goat anti-mouse IgG (#BE102, Beijing EASYBIO) were also purchased respectively.

2.13. Golgi staining

After rapid decapitation and execution, mouse brains were sorted, rinsed clean of blood with water, and then immersed in pre-configured Golgi staining solution before following the instructions of the Golgi Staining Kit (#PK401A, FD NeuroTechnologies, Inc.). Brain slices were photographed under a laser confocal microscope with an oil lens, and the density of dendritic spines was analysed with Image J software.

2.14. Transmission electron microscopy (TEM) sampling and imaging

Hippocampal tissue was isolated, cut into 1 mm^3 pieces with a sharp blade, placed in electron microscope fixative at 4 °C overnight, rinsed, post-fixed, dehydrated, embedded, sectioned (60 nm thick), and double-stained with 2 % uranyl acetate saturated alcoholic solution and lead citrate. The ultrastructure of the neurons were observed and photographed under a TEM.

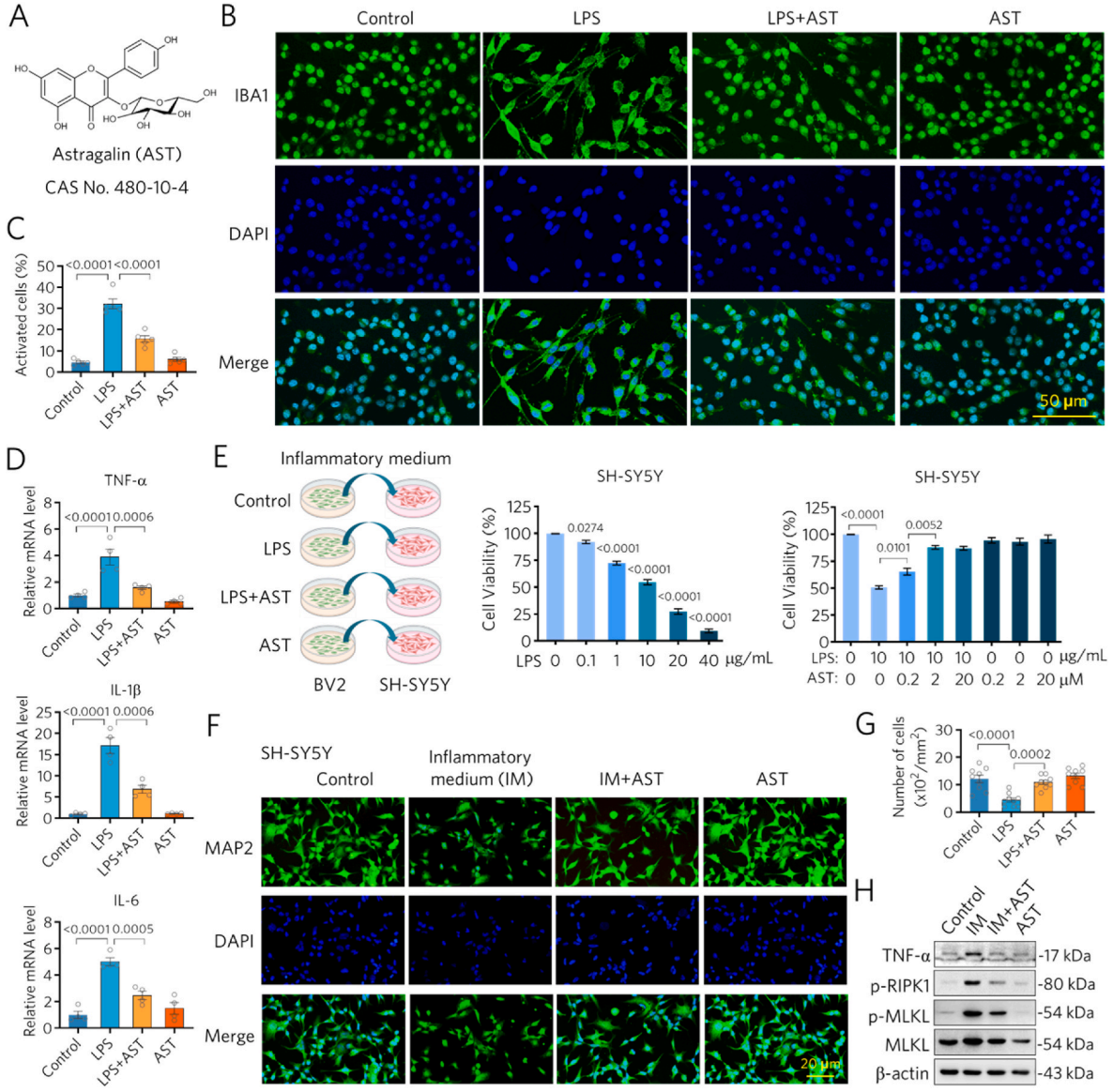

Fig. 1. AST inhibits LPS-induced inflammatory response and cell viability impairment. (A) Chemical structural formula of AST. (B) AST inhibited LPS-induced inflammatory activation and morphological changes in BV2 cells. BV2 cells treated with LPS exhibited elongated shapes, indicative of inflammatory activation, which was suppressed by AST. (C) Quantification of inflammation-activated cells in (B). (D) AST reversed the LPS-induced upregulation of pro-inflammatory factors TNF-α, IL-1β, and IL-6 at the mRNA level in BV2 cells. (E) Inflammatory medium (IM) generated from LPS-treated BV2 cells significantly reduced the viability of SH-SY5Y cells, an effect that was reversed by AST. AST alone showed no cytotoxicity. (F–G) Immunofluorescence staining revealed that IM significantly altered the morphology and reduced the number of SH-SY5Y cells. AST treatment attenuated these changes, preserving cell morphology and viability. (H) Western blot analysis showed that LPS treatment significantly altered protein levels of TNF-α and components of the RIPK1/MLKL signalling axis. AST restored these proteins to baseline levels. Data are shown as mean ± S.E.M and analysed by one-way ANOVA followed by Tukey's multiple comparisons test. Numerical p-values are shown.

2.15. Statistical analysis

Data are expressed as mean ± S.E.M. One-way analysis of variance (ANOVA) and Tukey's multiple comparison tests were used for comparisons. Non-parametric data were analysed using the Mann-Whitney test. GraphPad Prism 9.5.1 software was used for statistical analysis and graphing.

3. Results

3.1. AST protects cultured cells from LPS-induced inflammatory damage

To evaluate the anti-inflammatory effect of AST in cultured cells (Fig. 1), microglial BV2 cells were incubated with LPS and/or AST. Immunofluorescence staining for the microglial marker IBA1 revealed that LPS-treated BV2 cells underwent significant morphological changes ($p < 0.0001$, $df = 16$), exhibiting an elongated shape reminiscent of epithelial-mesenchymal transition, indicative of inflammatory activation (Fig. 1B and C). However, AST treatment suppressed these LPS-induced pro-inflammatory changes ($p < 0.0001$, $df = 16$) (Fig. 1B and C), while AST alone did not induce any observable alterations in BV2 cells. Furthermore, mRNA expression levels of classical pro-inflammatory factors, including TNF-α, IL-1β, and IL-6, confirmed that LPS triggered inflammatory activation in BV2 cells ($p < 0.0001$, $df = 12$), which was effectively inhibited by AST (Fig. 1D).

To further investigate, we collected the culture medium from BV2 cells treated with graded concentrations of LPS, termed inflammatory medium (IM), and applied it to SH-SY5Y cells after centrifugation to

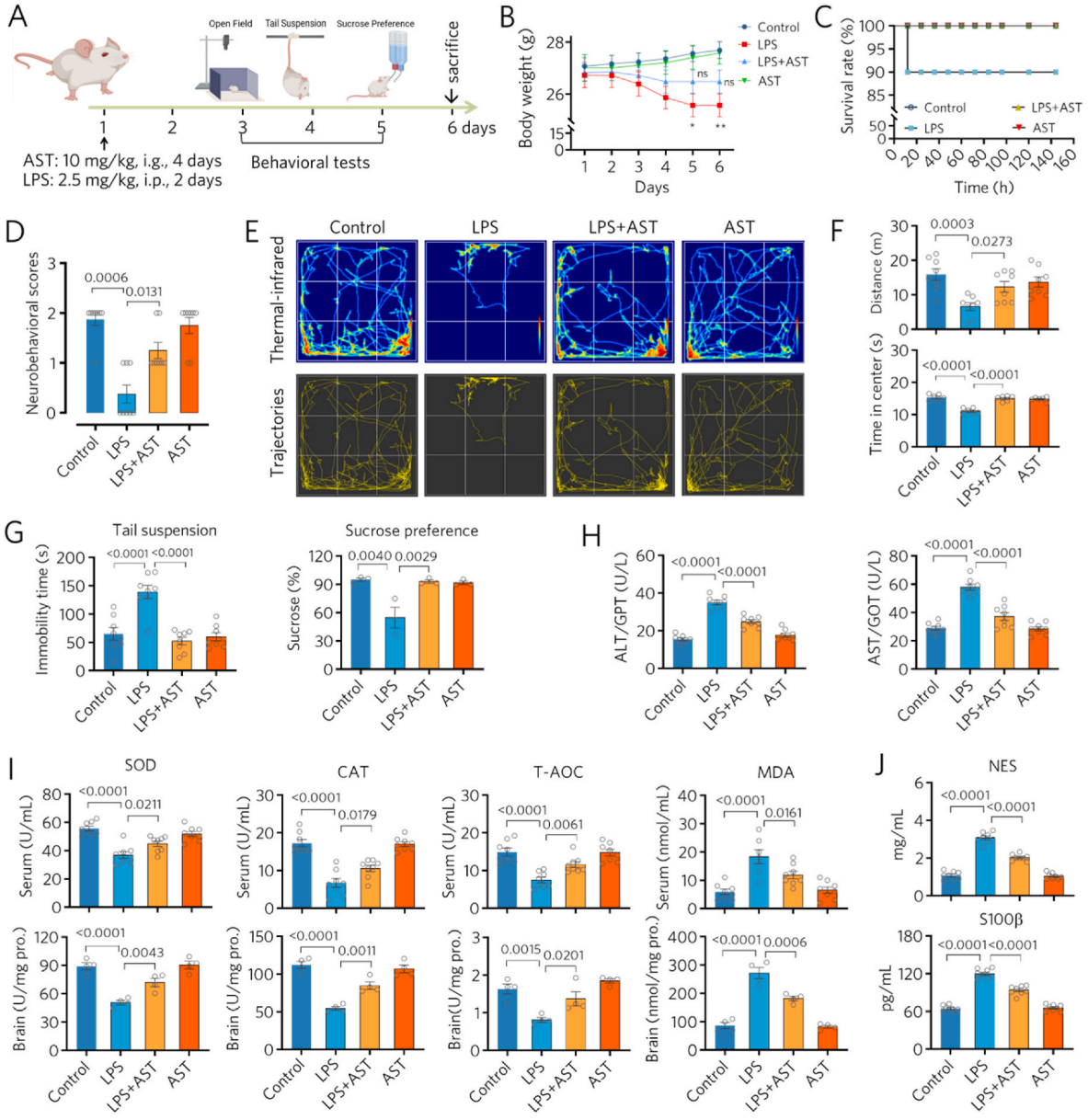

Fig. 2. AST attenuates LPS-induced depressive-like behaviour in mice. (A) Schematic diagram of the experimental procedure and behavioural tests. (B–C) AST (10 mg/kg body weight) rescued LPS (2.5 mg/kg body weight)-induced weight loss in mice and improved survival rates. *, $p < 0.05$; **, $p < 0.01$; n.s, not significant. (D) Neurobehavioral scores of mice assessed using the Mann-Whitney test. (E–F) Statistical analysis of mice trajectories in the OFT, including total distance travelled and time spent in the central region. (G) Results of the tail suspension test (TST) and sucrose preference test (SPT) in mice. (H) Serum levels of alanine aminotransferase (ALT) and aspartate aminotransferase (AST), indicating liver function. (I) Assays for oxidative stress indicators in serum and brain tissue. (J) ELISA results for serum markers of nerve injury, NSE and S100β. Data are expressed as mean ± S.E.M and analysed by one-way ANOVA and Tukey's multiple comparison tests except for (D); n.s indicates not significant.

remove cellular debris. The results demonstrated that IM from LPS-stimulated BV2 cells significantly reduced the viability of SH-SY5Y cells ($p < 0.0001$, $df = 24$), indicating that inflammatory factors released by BV2 cells inhibited SH-SY5Y cell activity (Fig. 1E). Using the optimal LPS concentration (10 μg/mL), we conducted cellular protection experiments with AST and found that AST significantly protected SH-SY5Y cells from IM-induced damage ($p = 0.0052$, $df = 32$ at AST = 2 μM) (Fig. 1E). Immunofluorescence imaging of SH-SY5Y cells stained with the neuronal marker MAP2 further confirmed that IM from LPS-treated BV2 cells markedly reduced SH-SY5Y cell activity and cell number ($p < 0.0001$, $df = 32$) (Fig. 1F). Conversely, AST attenuated IM-induced injury and maintained SH-SY5Y cell viability (Fig. 1G). Western blot analysis revealed that IM activated the expression of pro-inflammatory factors such as TNF-α and triggered the RIPK1/RIPK3/MLKL inflammatory signalling pathway in SH-SY5Y cells (Fig. 1H). In contrast, AST inhibited these changes and preserved cellular homeostasis (Fig. 1H). In summary, AST protected cells from LPS-induced inflammatory injury.

3.2. AST ameliorates LPS-induced depressive-like behaviour in mice

BALB/C mice were randomly divided into four groups: Control, LPS, LPS + AST, and AST groups, and treated as described in the "Materials and Methods" section, followed by behavioural tests (Fig. 2A). Mice treated with LPS (2.5 mg/kg body weight) showed a significant decrease in body weight on day 5 (*, $p = 0.0124$, $df = 12.68$) and day 6 (**, $p = 0.0089$, $df = 12.99$) compared to the control group. In contrast, mice co-treated with AST (LPS + AST group) showed only a slight decrease in body weight, with no significant difference compared to the control group ($p = 0.1819$, $df = 12.80$ at day 6) (Fig. 2B). In addition, mortality observations revealed that LPS-treated mice experienced deaths, whereas no deaths occurred in the LPS + AST and AST groups, suggesting that AST protects mice from LPS toxicity (Fig. 2C). Neurobehavioral assessments, including auricular reflex, tail pinch reflex, corneal reflex, escape reflex, and flip reflex, were also conducted. The results indicated that LPS-treated mice exhibited more severe neurological damage compared to the control group ($p = 0.0006$), while AST maintained normal neurobehavioral function in mice ($p = 0.0131$, LPS + AST vs AST) (Fig. 2D).

Subsequent behavioural tests, including the open field test (OFT), tail suspension test (TST), and sucrose preference test (SPT), were performed (Fig. 2E–G). LPS-treated mice displayed significantly reduced exploratory behaviour, motivation to escape restraint, and preference for sucrose water, indicative of depressive-like behaviours. In contrast, AST treatment alleviated these behavioural abnormalities, restoring mice to a normal state (Fig. 2E–G). AST alone did not induce any observable effects. Liver function tests revealed elevated transaminase levels (ALT/GPT and AST/GOT) in LPS-treated mice ($p < 0.0001$, $df = 28$), which were normalized by AST (Fig. 2H). Furthermore, redox indices in serum and brain tissues showed that LPS significantly decreased antioxidant regulators such as SOD, CAT, and T-AOC, while increasing the oxidative stress marker MDA (Fig. 2I). AST effectively regulated oxidative stress and restored homeostasis. ELISA measurements of serum NSE and S100β, specific markers of nerve injury, further confirmed that AST reduced neuronal damage (Fig. 2J). In conclusion, AST protected mice from LPS-induced oxidative and neurological damage, thereby mitigating depressive-like behavioural changes.

3.3. AST maintains BBB integrity and inhibits LPS-induced inflammatory damage

LPS-mediated disruption of the BBB is a critical event in the pathogenesis of brain diseases. To evaluate BBB integrity, we employed the Evans blue leakage assay (Fig. 3A). Brain tissue sections from control

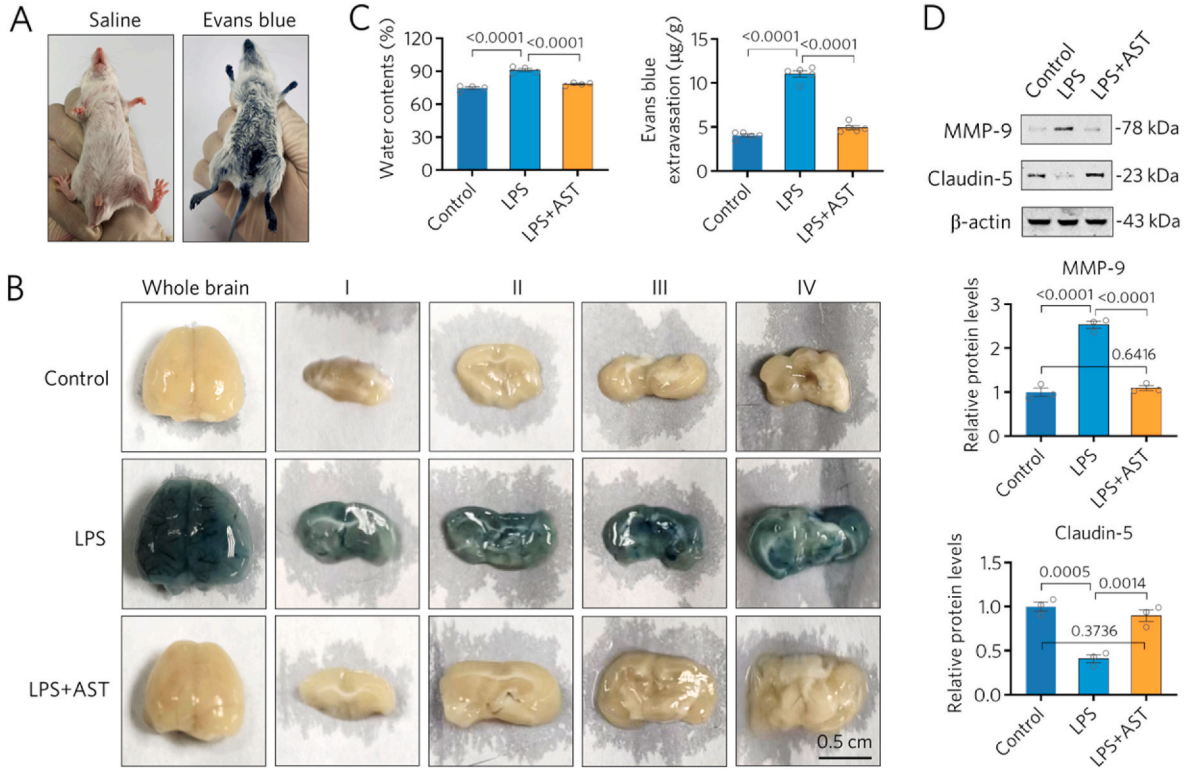

Fig. 3. AST protects the BBB from LPS-induced damage. (A–B) Representative images of mice and Evans blue (EB) staining in the brains. (C) Quantification of brain edema (water contents) and Evans blue staining index. (D) Representative Western blots of matrix metalloproteinase-9 (MMP-9) and the BBB tight junction marker Claudin-5. Relative expression levels were analysed based on band density (n = 3). Data are expressed as mean ± S.E.M and analysed by one-way ANOVA and Tukey's multiple comparison tests. (For interpretation of the references to colour in this figure legend, the reader is referred to the Web version of this article.)

mice showed minimal Evans blue staining, while LPS-treated mice exhibited intense staining, indicative of BBB disruption. In contrast, AST-treated mice displayed staining patterns comparable to controls. (Fig. 3B). These findings were supported by statistical results, which revealed that LPS administration significantly increased brain water content ($p < 0.0001$, $df = 9$) and Evans blue leakage ($p < 0.0001$, $df = 12$) (Fig. 3C). However, AST treatment effectively prevented cerebral edema and reduced Evans blue leakage (Fig. 3C). Additionally, Western blot analysis of BBB marker proteins MMP-9 and Claudin-5 revealed that LPS increased MMP-9 expression ($p < 0.0001$, $df = 6$) and decreased Claudin-5 expression ($p = 0.0005$, $df = 6$), indicating BBB damage. AST treatment reversed these changes, restoring BBB integrity (Fig. 3D). In summary, LPS-induced inflammation compromised BBB integrity and increased permeability, while AST protected the BBB and maintained its normal function.

3.4. AST protects neurons from LPS-induced dendritic spine and synaptic damage

Synapses are essential for neuronal communication, and depressive-like behaviours in mice are often associated with neuronal and synaptic damage, including dendritic spine loss and synaptic vesicle alterations. We first investigated MAP2, a marker protein of hippocampal neurons, using immunofluorescence staining. MAP2, localized in the cytosol, dendrites, dendritic spines, and postsynaptic regions, regulates synaptic plasticity and cytoskeletal dynamics. MAP2/DAPI staining in the hippocampal CA1 region revealed tightly arranged neurons with strong fluorescence in the control group, whereas LPS-treated mice showed reduced neuron numbers and nuclear fragmentation (Fig. 4A). AST treatment restored MAP2 staining and neuron numbers to control levels (Fig. 4A). We further examined the protrusions of neurons in the CA1

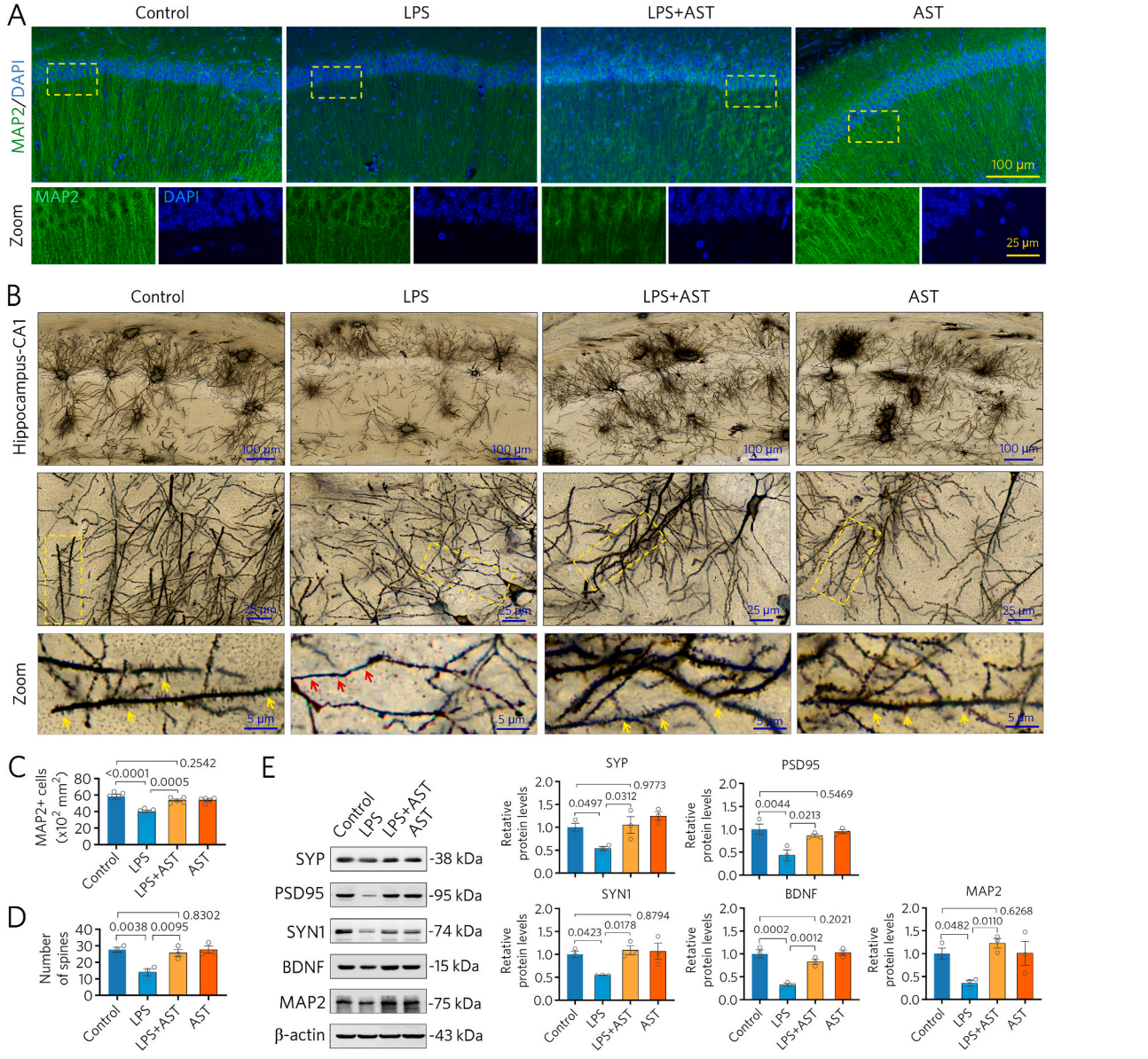

Fig. 4. AST inhibits LPS-induced neuronal damage and dendritic spine loss. (A) Representative immunofluorescence images of MAP2 (green) staining in the CA1 region of the hippocampus. DAPI staining indicates nuclei. (B) Golgi staining of neuronal axons and dendritic spines. Yellow arrows highlight intact dendritic spines in the control and AST-treated groups, while red arrows indicate dendritic spine loss in LPS-treated mice. (C–D) Statistical analysis of the number of MAP2-positive cells and dendritic spines. (E) Western blot analysis and quantification of protein levels of synaptophysin (SYP), postsynaptic density protein 95 (PSD95), synapsin-1 (SYN1), BDNF, and neuronal marker MAP2. Relative expression levels were normalized to β-actin (n = 3). Data are expressed as mean ± S.E.M and analysed by one-way ANOVA and Tukey's multiple comparison tests. (For interpretation of the references to colour in this figure legend, the reader is referred to the Web version of this article.)

area by Golgi staining (Fig. 4B), and found that neuronal dendritic spines in the control group were heavily interspersed in a reticulated pattern, and the protrusions were clustered at the edges of the dendrites in a punctate pattern, while LPS-treated mice exhibited fragmented dendrites and reduced spine density (Fig. 4B–LPS). However, AST treatment inhibited LPS disruption and restored dendritic spine morphology (Fig. 4B–LPS + AST). Statistical analyses of MAP2-positive cells and dendritic spine protrusions also corroborated these findings (Fig. 4C and D). At the molecular level, we also detected MAP2, BDNF, and synaptic function marker proteins such as SYP, PSD95 and SYN1. The results showed that the expression of all the above proteins was reduced to different degrees in the LPS-mediated neuronal injury group, but AST restored them (Fig. 4E). These results suggest that AST protects neuronal plasticity from LPS-induced damage.

3.5. AST protects brain tissue from LPS-induced mitochondrial and synaptic damage

We further observed the morphological changes of synaptic vesicles and mitochondria in neurons at the subcellular level by TEM (Fig. 5). Normal neurons had clear cell membrane boundaries at synaptic sites with vesicles stacked nearby; mitochondrial cristae were also clearly visible (Fig. 5, Control). In contrast, LPS-treated neurons exhibited blurred synaptic membranes, disrupted vesicle morphology, and fragmented mitochondrial cristae (Fig. 5, LPS). AST treatment restored synaptic and mitochondrial structures to normal (Fig. 5, LPS + AST). Statistical analyses confirmed that LPS reduced presynaptic vesicles ($p = 0.0021$, $df = 16$), while AST reversed these effects. The same was true for damage and recovery of mitochondrial cristae. These findings indicate that AST protects synaptic and mitochondrial structures from LPS-induced damage.

3.6. AST inhibits LPS-induced inflammatory activation of glial cells and enhances glycolytic pathway activity

Having confirmed the neuronal damage caused by LPS-induced inflammatory response, we further investigated the mechanisms underlying LPS-induced inflammatory damage by examining glial cell activation and glycolytic pathway activity in brain tissue. Immunofluorescence staining for glial markers IBA1 (microglia) and GFAP

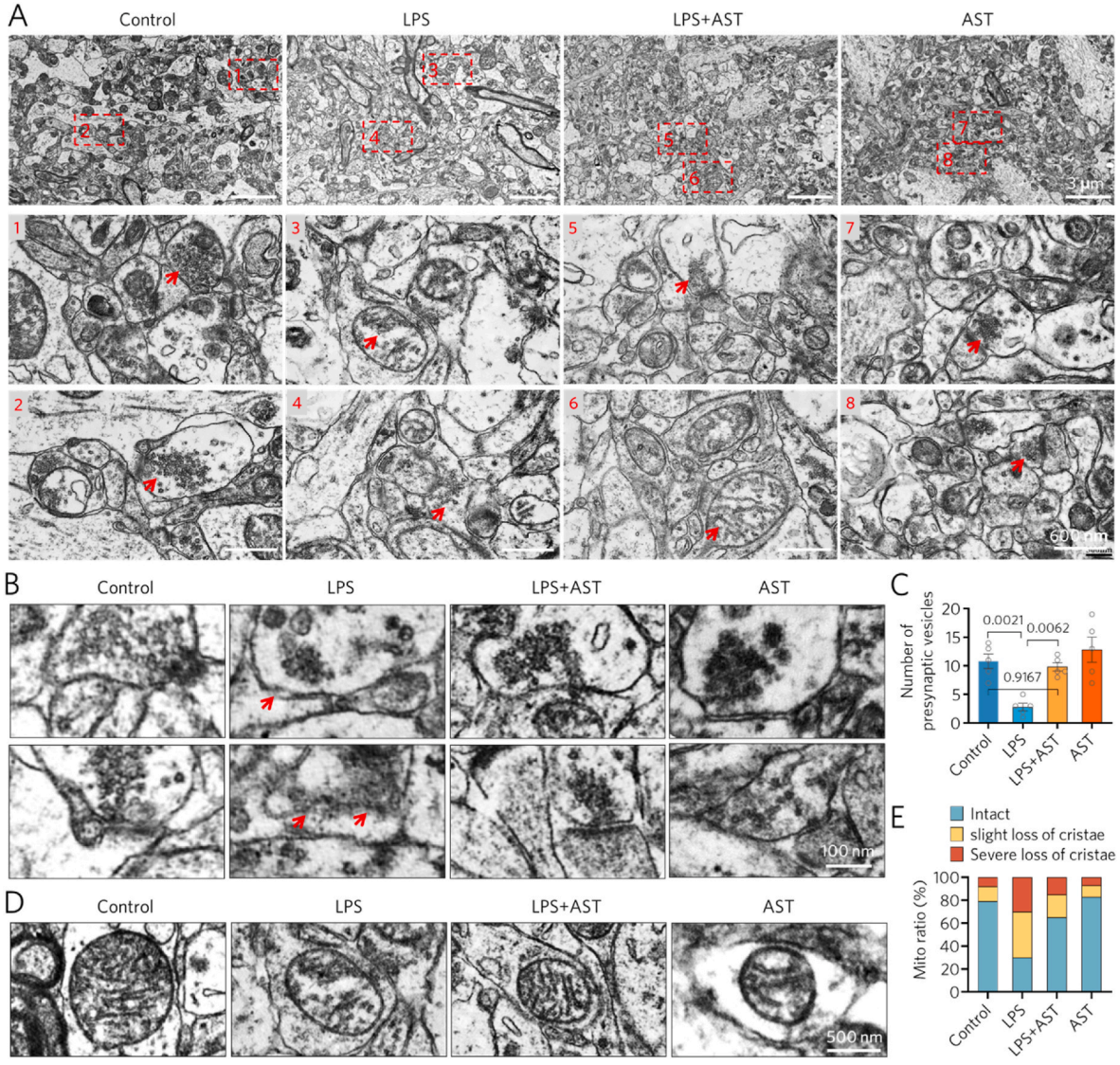

Fig. 5. AST protects brain from LPS-induced mitochondrial and synaptic damage. (A) Representative TEM image of the hippocampal CA1 region. Arrows indicate mitochondria and synapses. (B) Magnified TEM images of synapses and synaptic vesicles. Arrows highlight damaged presynaptic membranes in LPS-treated mice. (C) Quantification of the number of presynaptic vesicles. (D) Magnified TEM images of mitochondria. LPS-treated mice exhibited severe cristae deletion, which was rescued by AST. (E) Quantification of mitochondrial phenotypes. Data are analysed by one-way ANOVA and Tukey's multiple comparison tests.

(astrocytes) revealed that LPS significantly increased the expression of these markers, indicating robust glial cell activation (Fig. 6). Quantitative analysis showed that the expression of IBA1 ($p = 0.0023$, $df = 20$), which represents microglia, and GFAP ($p < 0.0001$, $df = 20$), which represents astrocytes, was significantly enhanced in LPS-treated brain tissues, accompanied by an increase in the number of IBA1- and GFAP-positive cells. These results suggest that LPS triggers a pronounced inflammatory response in brain tissue, characterized by glial cell activation (Fig. 6, LPS). Additionally, we observed a significant upregulation of PKM2 ($p < 0.0001$, $df = 20$), a key kinase in the glycolytic pathway, in LPS-treated brain tissues (Fig. 6, LPS). The enhanced glycolytic activity likely supports the energy demands of activated glial cells during inflammatory responses. In contrast, AST treatment restored the expression levels of IBA1, GFAP, and PKM2 to levels comparable to those in the control group (Fig. 6, LPS + AST).

In addition, we investigated changes in other relevant proteins involved in the glycolytic pathway, as well as lactate and ATP. We found that LPS induced an increase in the activities of HK and PK and a decrease in PDH activity in the glycolytic pathway, suggesting that the enhancement of glycolysis was accompanied by an increase in lactate production and a decrease in ATP production (Fig. 7A–LPS). RT-qPCR showed that the expression levels of genes related to the glycolytic pathway were also up-regulated, and confirmed the up-regulation of the expression of glucose transporters Glut1 and HK2, PKM2, LDHA, and HIF-1α. AST treatment restored the glucose metabolic homeostasis of brain tissue cells, i.e., the activity of the glycolytic pathway was restored to the level of the normal group (Fig. 7A–AST). These results indicate that AST attenuates LPS-induced glial cell activation and normalizes

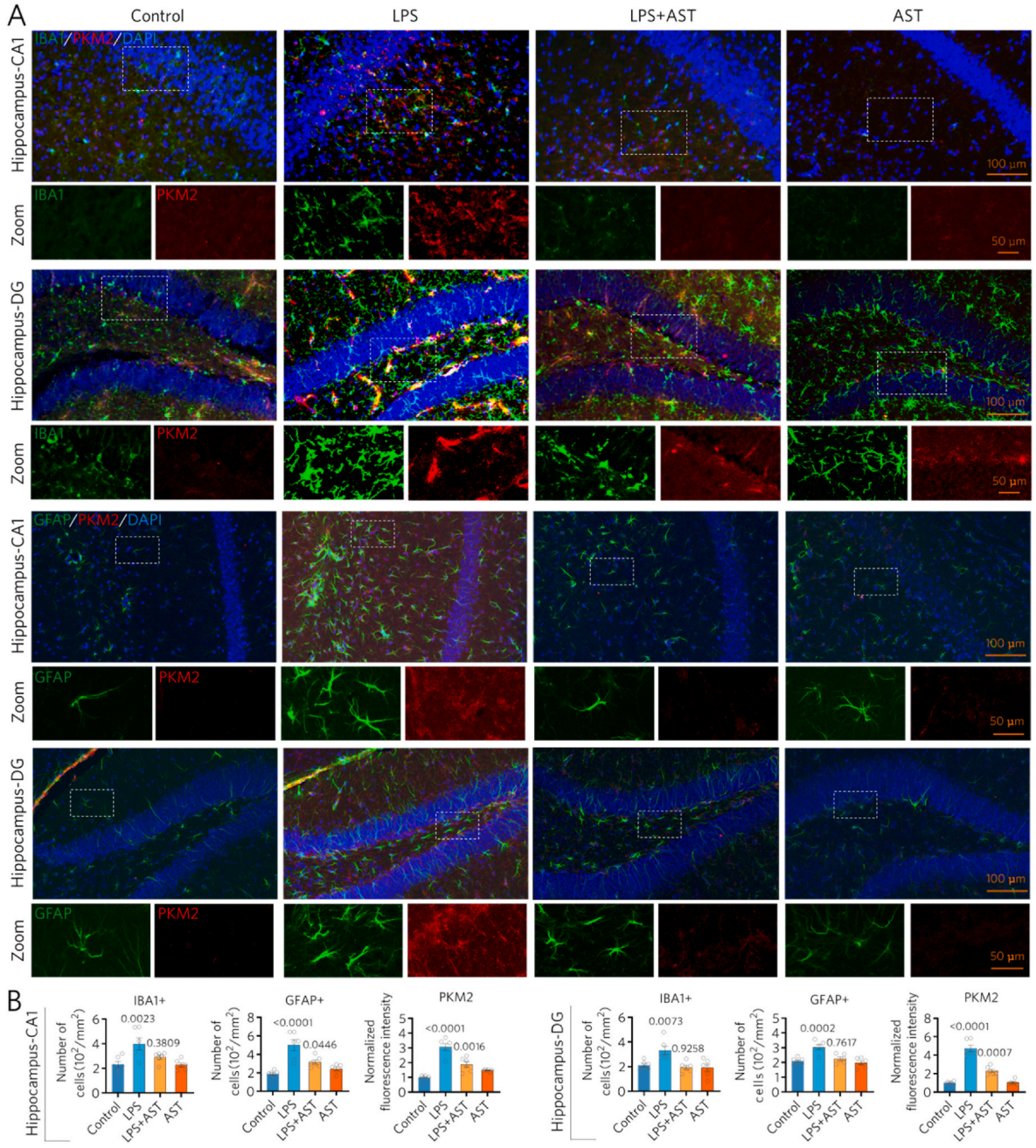

Fig. 6. AST attenuates LPS-induced glial cell activation and enhancement of glycolytic signalling. (A) Representative immunofluorescence images of IBA1 and GFAP (markers of glial cells) in the hippocampal CA1 region and dentate gyrus (DG), along with PKM2, a key glycolytic enzyme. (B) Quantification of IBA1- and GFAP-positive cells and PKM2 expression levels based on fluorescence intensity (n = 6).

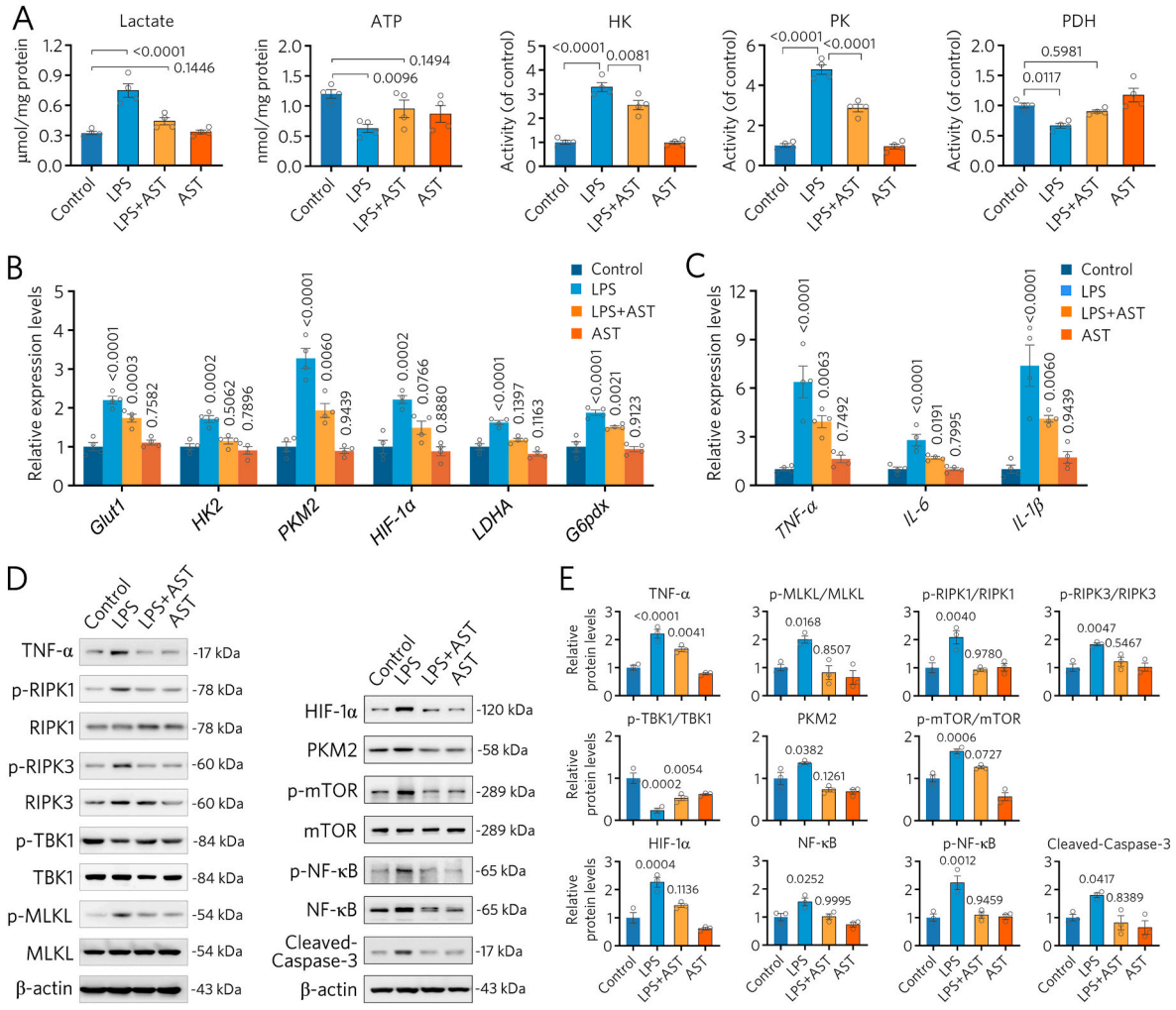

Fig. 7. AST inhibits LPS-induced enhancement of glycolysis and activation of RIPK1/RIPK3/MLKL and mTOR/NF-κB signalling axes. (A) ATP levels and activities of glycolytic enzymes (HK, PK, PDH), as well as lactate production, were measured. (B–C) RT-qPCR analysis of mRNA expression levels of genes involved in the glycolytic pathway and pro-inflammatory factors (TNF-α, IL-1β, IL-6) in brain tissue (n = 4). (D–E) Western blot analysis and quantification of protein levels in the mTOR/NF-κB and RIPK1/RIPK3/MLKL signalling pathways (n = 3). Data are shown as mean ± SEM and analysed by one-way ANOVA followed by Tukey's multiple comparisons tests.

glycolytic pathway activity, thereby mitigating neuroinflammation and its associated metabolic dysregulation.

3.7. AST inhibits activation of inflammatory signalling pathways, including RIPK1/RIPK3/MLKL, to prevent inflammatory damage to neurons

We investigated the molecular mechanisms underlying LPS-induced inflammation by analysing the expression of pro-inflammatory factors and signalling pathways (Fig. 7). RT-qPCR revealed that LPS significantly upregulated TNF-α, IL-6, and IL-1β expression ($p < 0.0001$) (Fig. 7C–LPS), which was inhibited by AST (Fig. 7C–LPS + AST). Western blot analysis showed that LPS increased the levels of RIPK1, RIPK3, MLKL, and their phosphorylated forms, indicating activation of the RIPK1 signalling axis, while decreasing the expression of the endogenous inhibitor TBK1 (Fig. 7D–LPS). AST treatment reversed these changes, restoring signalling pathway activity to control levels (Fig. 7D–LPS + AST). Similarly, LPS activated the mTOR/NF-κB signalling axis, which was normalized by AST (Fig. 7D). Statistical analyses of Western blot results confirmed these findings (Fig. 7E). In summary, LPS induced inflammatory responses and activated inflammatory signalling pathways in brain tissue, while AST effectively inhibited these pro-inflammatory effects.

We confirmed the LPS-induced inflammatory response and its damage to neuronal cells in cultured cells and mouse models in vitro, and then AST successfully reversed all these LPS damages to neuronal cells (Fig. 8). In other words, AST was able to protect the integrity of the BBB from LPS invasion into the brain tissue and caused excessive inflammation and its associated signalling pathway activation and enhanced glycolysis. Therefore, AST has the potential to be used in the development of BBB-targeted drugs.

4. Discussion

In clinical settings, severe trauma or infections can lead to systemic inflammatory response syndrome or sepsis, often resulting in multi-organ dysfunction. Pathogenic factors such as LPS and inflammatory cytokines (e.g., TNF-α, IL-1β, IL-6) can breach the BBB through the blood circulation, triggering neuroglial activation, mitochondrial dysfunction, and SAE. SAE, prevalent in intensive care units, has an incidence of approximately 70 % among sepsis patients, with a mortality rate of 56.1 %, compared to 35.1 % in sepsis patients without SAE [2]. Survivors often experience long-term cognitive impairments, highlighting the need for therapies with dual anti-inflammatory and neuroprotective effects [24]. Therefore, research on drugs with dual anti-inflammatory and neuroprotective effects has become more urgent. Flavonoids and

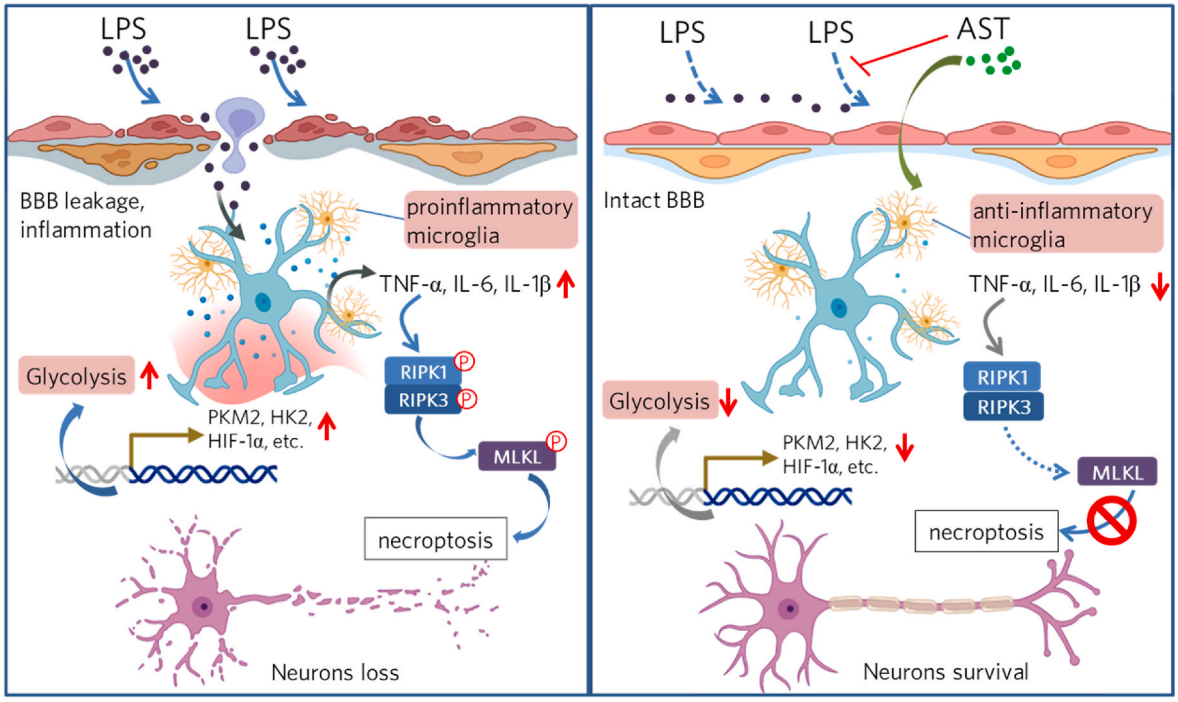

Fig. 8. The schematic diagram illustrates AST's protective effects against LPS-induced BBB damage and its mechanisms.
LPS disrupts BBB integrity, leading to leakage and triggering a pronounced inflammatory response in the brain. This includes glial cell activation, elevated expression of pro-inflammatory factors (e.g., TNF-α, IL-1β, IL-6), aberrant glucose metabolism, and activation of inflammatory signaling pathways such as RIPK1/RIPK3/MLKL. These changes result in synaptic damage and neuronal death. AST alleviates LPS-induced toxicity and pro-inflammatory responses, maintaining BBB integrity and CNS homeostasis.

glycosides, widely present in natural products, demonstrate anti-inflammatory, antioxidant, and antimicrobial activities, making them promising candidates for neuroprotection. AST has demonstrated antidepressant effects through mechanisms such as anti-inflammation, oxidative stress inhibition, sedation, and neuroprotection. AST reduces the expression of pro-inflammatory mediators (e.g., iNOS, COX-2) in LPS-treated macrophages by inhibiting the activation of NF-κB, a key regulator of inflammation [14,25]. Additionally, AST upregulates SIRT1 expression and modulates its mediated signalling pathway to suppress NLRP3 inflammasome activity, thereby exerting anti-inflammatory and neuroprotective effects [26]. In mouse models, AST exhibits sedative and hypnotic effects, mitigating depressive symptoms by promoting relaxation and sleep [27]. AST also promotes M2 polarization of glial cells by regulating the IL-4R/JAK1/STAT6 signalling pathway to attenuate depression-like behaviors and memory deficits [14]. These findings collectively support the multi-target and multi-pathway mechanisms underlying the antidepressant effects of AST.

Our previous studies have shown that AST mitigates chemical toxicity (e.g., $AlCl_3$+D-galactose-induced brain damage) and improves learning and memory deficits caused by neuronal injury [15]. Other natural compounds, such as CE (active components of Tibetan ginseng glycosides), salidroside, and paeoniflorin, also exhibit neuroprotective effects by inhibiting inflammation and apoptosis, improving behaviours in models of Alzheimer's disease, Parkinson's disease, and depression [28–32]. Building on these findings, we investigated the protective effects of AST on BBB and its underlying mechanisms. In the LPS-treated mouse model, the BBB was severely compromised, as evidenced by brain edema and dysregulated expression of BBB-associated proteins, such as increased MMP-9 and decreased Claudin-5 levels (Fig. 3). This disruption facilitated the infiltration of LPS and pro-inflammatory factors into brain tissue, triggering neuroinflammation and neuronal damage. For example, MAP2, a cytoskeletal protein localized in neuronal cell bodies, dendrites, and postsynaptic regions, was significantly reduced in LPS-treated mice, indicating neuronal loss (Fig. 4). Furthermore, dendritic spines, synapses, and mitochondria were damaged (Fig. 5), directly impairing neuronal function and contributing to behavioral deficits. These observations align with previous studies demonstrating that LPS activates the TLR4-NF-κB and MAPK signalling pathways, promoting the expression of inflammatory cytokines (e.g., TNF-α, IL-1β) and reactive oxygen species (ROS) production, which directly contribute to synaptic and mitochondrial damage [33]. Notably, AST treatment effectively protected BBB integrity, attenuated neuroinflammation, and prevented neuronal and mitochondrial damage (Figs. 3–5). These findings suggest that AST exerts its neuroprotective effects by modulating inflammatory and oxidative stress pathways, thereby preserving neuronal structure and function.

On the other hand, the inflammatory response activated by LPS brings about profound cellular changes as well as shifts in the pattern of energy metabolism in glial cells of brain tissue. Resting microglia can polarise to either pro-inflammatory phenotype M1 or an anti-inflammatory phenotype M2 in response to different stimuli, and their energy metabolism tends to shift from oxidative phosphorylation to glycolysis, accompanied by elevated expression of glucose transporter protein type 1 (Glut1) to increase glucose uptake [34]. Pyruvate kinase (PK) is one of the key enzymes of glycolysis, which generates pyruvate and ATP by catalysing the transfer of a phosphate from phosphoenolpyruvate (PEP) to ADP, thus enabling rapid cellular access to ATP. PKM2 is also the rate-limiting enzyme in the regulation of glycolysis [35]. PKM2 exists in tetrameric and dimeric forms, which are inter-convertible and have different biological activities [36,37]. Under normal conditions, PKM2 exists mainly in the form of tetramers and exhibits active pyruvate kinase activity (metabolic enzyme activity) in the cytoplasm. Upon stimulation, PKM2 mainly exhibits protein kinase activity and transfers to the nucleus as a dimer, thereby regulating the transcription and expression of downstream genes. The current study suggests that PKM2 appears to be a key regulator of the expression and secretion of pro-inflammatory molecules. Inhibition of PKM2 nuclear translocation and complexation of PKM2 with hypoxia -inducible

factor-1α (HIF-1α) has been reported to inhibit hepatic inflammation. HIF-1α is recruited to the hypoxia-response element sites to form the HIF-1α-PKM2 complex, which enhances the nuclear translocation of PKM2 as a dimer and phosphorylates the nuclear transcription factor STAT3, which promotes the production of the pro-inflammatory factor IL-1β [38]. The inflammatory response-induced increase in HIF-1α expression is considered to be a key molecule in the transition from OXPHOS to aerobic glycolysis in inflammatory cells, which activates the transcription of glucose metabolism-related genes and promotes glycolysis, in contrast to the marked inhibition of intracellular oxidative phosphorylation. We observed the above changes in the LPS-induced mouse model, i.e., up-regulation of PKM2 expression and activity, and the up-regulation of HIF-1α, Glut1, IL-1β, etc., which confirmed the LPS-induced inflammatory response and changes in cellular energy metabolism. However, AST inhibited the pro-inflammatory activity of LPS and maintained CNS homeostasis. Similarly, activation or inhibition of the RIPK1/RIPK3/MLKL inflammatory signalling pathway as well as the mTOR/NF-κB axis occurred during LPS or AST treatments (Fig. 7). In other words, maintaining the integrity of the BBB and suppressing the inflammatory response induced by pathogenic factors such as LPS can keep glial cells and neurons in a normal functional state (Fig. 8).

5. Conclusions

We demonstrated that AST inhibits LPS-induced inflammatory activation in BV2 cells and protects SH-SY5Y cells from inflammatory injury. AST ameliorates LPS-induced depressive-like behaviours in mice by preserving BBB integrity and inhibiting neuroinflammation. LPS activates the glycolytic pathway and inflammatory signalling pathways (RIPK1/RIPK3/MLKL, mTOR/NF-κB), while AST restores these pathways to maintain CNS homeostasis. These findings highlight AST's potential as a therapeutic agent for BBB-targeted drug development.

CRediT authorship contribution statement

Min-Min Cao: Methodology, Investigation, Data curation. **Zhe Guo:** Visualization, Methodology, Funding acquisition. **Jun Wang:** Validation, Software, Investigation. **Hui-Yong Ma:** Validation, Investigation. **Xiao-Yan Qin:** Visualization, Supervision, Project administration, Funding acquisition. **Yang Hu:** Validation, Supervision, Methodology. **Rongfeng Lan:** Writing – review & editing, Writing – original draft, Supervision.

Data availability

Datasets generated during and/or analysed during the current study are available from the corresponding author on reasonable request.

Declaration of competing interest

The authors declare that they have no known competing financial interests or personal relationships that could have appeared to influence the work reported in this paper.

Acknowledgements

This study was supported by the Academic Team Leadership Program of Minzu University of China (2023QNYL16, 2024XSYL02) and the Scientific Research Program of Guangxi Administration of Traditional Chinese Medicine (GXZYA20240474).

References

[1] L. Zhao, Y. Gao, S. Guo, X. Lu, S. Yu, Z.Z. Ge, H.D. Zhu, Y. Li, Sepsis-associated encephalopathy: insight into injury and pathogenesis, CNS Neurol. Disord.: Drug Targets 20 (2) (2021) 112–124.
[2] T.E. Gofton, G.B. Young, Sepsis-associated encephalopathy, Nat. Rev. Neurol. 8 (10) (2012) 557–566.
[3] Q. Liu, J.N. Zhao, Z.T. Fang, X. Wang, B.G. Zhang, Y. He, R.J. Liu, J. Chen, G.P. Liu, BGP-15 alleviates LPS-induced depression-like behavior by promoting mitophagy, Brain Behav. Immun. 119 (2024) 648–664.
[4] J.C. O'Connor, M.A. Lawson, C. Andre, M. Moreau, J. Lestage, N. Castanon, K. W. Kelley, R. Dantzer, Lipopolysaccharide-induced depressive-like behavior is mediated by indoleamine 2,3-dioxygenase activation in mice, Mol. Psychiatr. 14 (5) (2009) 511–522.
[5] R. Dantzer, J.C. O'Connor, G.G. Freund, R.W. Johnson, K.W. Kelley, From inflammation to sickness and depression: when the immune system subjugates the brain, Nat. Rev. Neurosci. 9 (1) (2008) 46–56.
[6] W.A. Banks, M.A. Erickson, The blood-brain barrier and immune function and dysfunction, Neurobiol. Dis. 37 (1) (2010) 26–32.
[7] Z. Peng, X. Li, J. Li, Y. Dong, Y. Gao, Y. Liao, M. Yan, Z. Yuan, J. Cheng, Dlg1 knockout inhibits microglial activation and alleviates lipopolysaccharide-induced depression-like behavior in mice, Neurosci. Bull. 37 (12) (2021) 1671–1682.
[8] C. Wei, W. Jiang, R. Wang, H. Zhong, H. He, X. Gao, S. Zhong, F. Yu, Q. Guo, L. Zhang, L.D.J. Schiffelers, B. Zhou, M. Trepel, F.I. Schmidt, M. Luo, F. Shao, Brain endothelial GSDMD activation mediates inflammatory BBB breakdown, Nature 629 (8013) (2024) 893–900.
[9] H. Du, S. Wang, Omarigliptin mitigates lipopolysaccharide-induced neuroinflammation and dysfunction of the integrity of the blood-brain barrier, ACS Chem. Neurosci. 11 (24) (2020) 4262–4269.
[10] D. Moujalled, A. Strasser, J.R. Liddell, Molecular mechanisms of cell death in neurological diseases, Cell Death Differ. 28 (7) (2021) 2029–2044.
[11] J. Yuan, P. Amin, D. Ofengeim, Necroptosis and RIPK1-mediated neuroinflammation in CNS diseases, Nat. Rev. Neurosci. 20 (1) (2019) 19–33.
[12] J. Chen, K. Zhong, S. Qin, Y. Jing, S. Liu, D. Li, C. Peng, Astragalin: a food-origin flavonoid with therapeutic effect for multiple diseases, Front. Pharmacol. 14 (2023) 1265960.
[13] C.Z. Yang, S.H. Wang, R.H. Zhang, J.H. Lin, Y.H. Tian, Y.Q. Yang, J. Liu, Y.X. Ma, Neuroprotective effect of astragalin via activating PI3K/Akt-mTOR-mediated autophagy on APP/PS1 mice, Cell Death Dis. 9 (1) (2023) 15.
[14] G. Yao, Z. Bai, J. Niu, R. Zhang, Y. Lu, T. Gao, H. Wang, Astragalin attenuates depression-like behaviors and memory deficits and promotes M2 microglia polarization by regulating IL-4R/JAK1/STAT6 signaling pathway in a murine model of perimenopausal depression, Psychopharmacology (Berl) 239 (8) (2022) 2421–2443.
[15] Y. Hu, X. Fang, J. Wang, T.T. Ren, Y.Y. Zhao, J.F. Dai, X.Y. Qin, R.F. Lan, Astragalin attenuates AlCl3/D-galactose-induced aging-like disorders by inhibiting oxidative stress and neuroinflammation, Neurotoxicology 91 (2022) 60–68.
[16] M.M. Cao, Z. Guo, Y.T. Lu, S.J. Zhong, H.Y. Ma, M.H. Liu, X.Y. Qin, Y. Hu, C. Cao, Astragalin protects against lipopolysaccharide-triggered acute liver injury through suppression of necroptosis and inflammation and improvement of energy metabolism, J. Funct.Foods 118 (2024) 106298.
[17] A. Kumar, A. Singh, Ekavali, A review on Alzheimer's disease pathophysiology and its management: an update, Pharmacol. Rep. 67 (2) (2015) 195–203.
[18] J. Liu, R. Feng, D. Wang, T. Huo, H. Jiang, Triclosan-induced glycolysis drives inflammatory activation in microglia via the Akt/mTOR/HIF 1alpha signaling pathway, Ecotoxicol. Environ. Saf. 224 (2021) 112664.
[19] S. Zhou, Y. Li, Y. Hong, Z. Zhong, M. Zhao, Puerarin protects against sepsis-associated encephalopathy by inhibiting NLRP3/Caspase-1/GSDMD pyroptosis pathway and reducing blood-brain barrier damage, Eur. J. Pharmacol. 945 (2023) 175616.
[20] A.K. Kraeuter, P.C. Guest, Z. Sarnyai, The open field test for measuring locomotor activity and anxiety-like behavior, Methods Mol. Biol. 1916 (2019) 99–103.
[21] J.F. Cryan, C. Mombereau, A. Vassout, The tail suspension test as a model for assessing antidepressant activity: review of pharmacological and genetic studies in mice, Neurosci. Biobehav. Rev. 29 (4–5) (2005) 571–625.
[22] V. Zeldetz, D. Natanel, M. Boyko, A. Zlotnik, H.N. Shiyntum, J. Grinshpun, D. Frank, R. Kuts, E. Brotfain, J. Peiser, A new method for inducing a depression-like behavior in rats, J. Vis. Exp. 132 (2018).
[23] M. Radu, J. Chernoff, An in vivo assay to test blood vessel permeability, J. Vis. Exp. 73 (2013) e50062.
[24] L. Molnar, B. Fulesdi, N. Nemeth, C. Molnar, Sepsis-associated encephalopathy: a review of literature, Neurol. India 66 (2) (2018) 352–361.
[25] E.H. Kim, Y.Y. Shim, H.I. Lee, S. Lee, M.J.T. Reaney, M.J. Chung, Astragalin and isoquercitrin isolated from aster scaber suppress LPS-induced neuroinflammatory responses in microglia and mice, Foods 11 (10) (2022).
[26] Y. Tong, H. Fu, C. Xia, W. Song, Y. Li, J. Zhao, X. Zhang, X. Gao, J. Yong, Q. Liu, C. Yang, H. Wang, Astragalin exerted antidepressant-like action through SIRT1 signaling modulated NLRP3 inflammasome deactivation, ACS Chem. Neurosci. 11 (10) (2020) 1495–1503.
[27] X. Li, Z. Tang, D. Fei, Y. Liu, M. Zhang, S. Liu, Evaluation of the sedative and hypnotic effects of astragalin isolated from Eucommia ulmoides leaves in mice, Nat. Prod. Res. 31 (17) (2017) 2072–2076.
[28] J.P. Bai, J. Wang, Y. Hu, Q. Huang, J.F. Dai, G.L. Xiao, H.J. Yu, X.Y. Qin, R.F. Lan, Network pharmacological analysis of the active molecules in Coeloglossum viride var. bacteatum and their anti-Alzheimer's disease activity through restoration of energy metabolism and inhibition of inflammation, Arab. J. Chem. 16 (8) (2023).
[29] J.Y. Yang, J. Wang, Y. Hu, D.Y. Shen, G.L. Xiao, X.Y. Qin, R.F. Lan, Paeoniflorin improves cognitive dysfunction, restores glutamate receptors, attenuates gliosis and maintains synaptic plasticity in cadmium-intoxicated mice, Arab. J. Chem. 16 (1) (2023).

[30] Y. Yu, X.Y. Lang, X.X. Li, R.Z. Gu, Q.S. Liu, R. Lan, X.Y. Qin, 2,3,5,4'-Tetrahydroxystilbene-2-O-beta-d-glucoside attenuates MPP+/MPTP-induced neurotoxicity in vitro and in vivo by restoring the BDNF-TrkB and FGF2-Akt signaling axis and inhibition of apoptosis, Food Funct. 10 (9) (2019) 6009–6019.
[31] X.M. Shu, Y. Hu, X. Fang, J. Wang, X.Y. Qin, R.F. Lan, Salidroside alleviates cadmium-induced toxicity in mice by restoring the notch/HES-1 and RIP1-driven inflammatory signaling axis, Inflamm. Res. 71 (5–6) (2022) 615–626.
[32] X.Y. Lang, Y. Hu, J.P. Bai, J. Wang, X.Y. Qin, R. Lan, Coeloglossum viride var. Bracteatum extract attenuates MPTP-induced neurotoxicity in vivo by restoring BDNF-TrkB and FGF2-Akt signaling Axis and inhibiting RIP1-driven inflammation, Front. Pharmacol. 13 (2022) 903235.
[33] R. Yirmiya, I. Goshen, Immune modulation of learning, memory, neural plasticity and neurogenesis, Brain Behav. Immun. 25 (2) (2011) 181–213.
[34] L. Liu, J. Tang, X. Liang, Y. Li, P. Zhu, M. Zhou, L. Qin, Y. Deng, J. Li, Y. Wang, L. Jiang, D. Huang, Y. Zhou, S. Wang, Q. Xiao, Y. Luo, Y. Tang, Running exercise alleviates hippocampal neuroinflammation and shifts the balance of microglial M1/M2 polarization through adiponectin/AdipoR1 pathway activation in mice exposed to chronic unpredictable stress, Mol. Psychiatr. 29 (7) (2024) 2031–2042.
[35] J.C. Alves-Filho, E.M. Palsson-McDermott, Pyruvate kinase M2: a potential target for regulating inflammation, Front. Immunol. 7 (2016) 145.
[36] Y. Zhang, H. Li, H. Mai, D. Luo, X. Ji, Z. Liu, S. Peng, X. Xu, Y. Zhang, R. Lan, H. Li, A responsive fluorescent probe for detecting and imaging pyruvate kinase M2 in live cells, Chem. Commun. 58 (45) (2022) 6494–6497.
[37] E.M. Palsson-McDermott, A.M. Curtis, G. Goel, M.A. Lauterbach, F.J. Sheedy, L. E. Gleeson, M.W. van den Bosch, S.R. Quinn, R. Domingo-Fernandez, D. G. Johnston, J.K. Jiang, W.J. Israelsen, J. Keane, C. Thomas, C. Clish, M. Vander Heiden, R.J. Xavier, L.A. O'Neill, Pyruvate kinase M2 regulates Hif-1alpha activity and IL-1beta induction and is a critical determinant of the warburg effect in LPS-activated macrophages, Cell Metab. 21 (1) (2015) 65–80.
[38] S. Le, H. Zhang, X. Huang, S. Chen, J. Wu, S. Chen, X. Ding, S. Chen, J. Zhao, H. Xu, J. Cui, Y. Zou, J. Yu, L. Jiang, J. Wu, P. Ye, J. Xia, PKM2 activator TEPP-46 attenuates aortic aneurysm and dissection by inhibiting NLRP3 inflammasome-mediated IL-1beta secretion, J. Cardiovasc. Pharmacol. Therapeut. 25 (4) (2020) 364–376.